# Central production of lepton-antilepton pairs and heavy quark composite states in hadron diffractive collisions at ultrahigh energies

V.V. Anisovich[+], M.A. Matveev[+], V.A. Nikonov[+◇], J. Nyiri[*]

October 11, 2018

[+]*National Research Centre "Kurchatov Institute", Petersburg Nuclear Physics Institute, Gatchina, 188300, Russia*

◇ *Helmholtz-Institut für Strahlen- und Kernphysik, Universität Bonn, Germany*

* *Institute for Particle and Nuclear Physics, Wigner RCP, Budapest 1121, Hungary*

## Abstract

Central production of lepton-lepton pairs ($e^+e^-$ and $\mu^+\mu^-$) and heavy quark composite states (charmonia and bottomonia) in diffractive proton collisions (proton momenta transferred $|\mathbf{q}_\perp| \sim m/\ln s$) are studied at ultrahigh energies ($\ln s >> 1$), where $\sigma_{tot}(pp^\pm) \sim \ln^N s$ with $1 \lesssim N \lesssim 2$. The $pp^\pm$-rescattering corrections, which are not small, are calculated in terms of the $K$-matrix approach modified for ultrahigh energies. Two versions of hadron interactions are considered in detail: the growth (i) $\sigma_{tot}(pp^\pm) \sim \ln^2 s$, $\sigma_{inel}(pp^\pm) \sim \ln^2 s$ within the black disk mode and (ii) $\sigma_{tot}(pp^\pm) \sim \ln^2 s$, $\sigma_{inel}(pp^\pm) \sim \ln s$ within the resonant disk mode. The energy behavior of the diffractive production processes differs strongly for these modes, thus giving a possibility to distinguish between the versions of the ultrahigh energy interactions.

## 1   Introduction

Recent measurements of the total, elastic and inelastic $pp$ cross sections at the LHC [1, 2, 3, 4], and at cosmic ray energies by the Auger experiment [5], reveal a successive step towards ultrahigh energy hadron physics. For $\sigma_{tot}(pp^\pm)$, $\sigma_{el}(pp^\pm)$ and $\sigma_{inel}(pp^\pm)$ the data demonstrate a steady growth of the type $\ln^N s$ with $1 \lesssim N \lesssim 2$, similar to that what was seen at preLHC energies [6], thus initiating a discussion about the asymptotic regime, see [7, 8, 9, 10, 11] and references therein. The data for the $pp$ diffractive scattering tell us that the black spot appears in the impact parameter space, $\mathbf{b}$. It can be an indication of the beginning of the black disk regime but for a definite confirmation a study of the diffractive cross sections at larger energies,
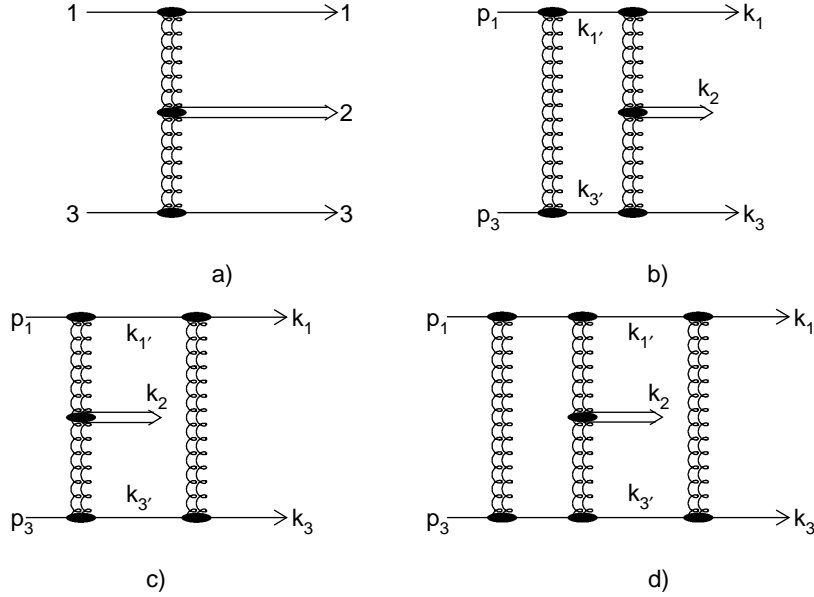
Figure 1: a) Input diagram for diffractive production $pp \to p(\ell\bar{\ell})p$ or $pp \to p(Q\bar{Q})p$ , and b), c), d) diagrams with subsequent rescatterings in initial and final states.

up to $\sqrt{s} \sim 10^4$ TeV [12], is required. The alternative can be the resonant mode, this regime starts also with a black spot at small $b$ [13].

In the search for and the recognition of asyptotics a study of diffractive production processes may be crucial. The principal point for the study of production processes at ultrahigh energies is to take into account the rescattering corrections which are large. The $K$-matrix technique modified for ultrahigh energies [14] give us the possibility to perform the corresponding calculations; we recall the main points of the technique in Section 2.

We study the central productions of lepton-lepton pairs ($\ell\bar{\ell} = e^+e^-, \mu^+\mu^-, ...$) and heavy quark states $Q\bar{Q} = J/\psi, \Upsilon$, and so on:

$$pp \to p(\ell\bar{\ell})p, \tag{1}$$
$$pp \to p(Q\bar{Q})p.$$

In these two reactions the centrally produced particles, leptons and heavy quarks, do not interact strongly with incoming and outgoing protons. But strong interactions of protons are to be taken into account. In Section 3, in the framework of the black disk and resonant disk modes for ultrahigh energy hadron interactions, we calculate amplitudes of processes (1).

## 2    Scattering amplitude and the $K(b)$-function

Diffractive scattering amplitudes at ultrahigh energies are usually considered in terms of the profile function $T(b)$ and the optical density $\chi(b)$. The $K$-matrix technique is convenient for studying the production processes, see [15] and references therein. We use the following notation:

$$\pi \frac{d\sigma_{el}}{d\mathbf{q}_\perp^2} = a^2(\mathbf{q}_\perp^2), \quad a(\mathbf{q}_\perp^2) = -\frac{1}{2} \int d^2\mathbf{b} \ e^{i\mathbf{b}\mathbf{q}_\perp} T(b), \tag{2}$$

2

$$T(b) = 1 - \eta(b)\, e^{2i\delta(b)} = 1 - e^{-\frac{1}{2}\chi(b)} = \frac{-2iK(b)}{1 - iK(b)} = -2a(\mathbf{b}^2, \ln s).$$

Here $b = |\mathbf{b}|$; in two-dimensional momenta transferred we omit the lower index $\perp$, i.e. $\mathbf{q}_\perp \to \mathbf{q}$; $a_{el}(\mathbf{q}_\perp^2)$ is the elastic scattering amplitude. The profile function can be presented either in the standard form using the inelasticity parameter $\eta(b)$ and the phase shift $\delta(b)$, or in terms of the optical density $\chi(b)$ and the $K$-matrix function $K(b)$. The $K$-matrix approach is based on the separation of the elastic rescatterings in the intermediate states: the function $K(b)$ includes only the multiparticle states thus being complex valued. The small value of the $ReA_{el}/ImA_{el}$ tells that $K(b)$ is dominantly imaginary.

## 2.1 Eikonal approach for scattering amplitude and the Feynman diagram technique

For the scattering amplitude of hadrons $A_{2\to2}\big((13)_{in} \to (13)_{out}\big)$ the reproducing integral reads:

$$A_{2\to2}\big((13)_{in} \to (13)_{out}\big) = K_{2\to2}\big((13)_{in} \to (13)_{out}\big) + \tag{3}$$

$$\int \frac{d^4 k_{3'}}{(2\pi)^4 i}\, A_{2\to2}\big((13)_{in} \to 1'3'\big) \frac{1}{(m^2 - k_{1'}^2 - i0)(m^2 - k_{3'}^2 - i0)}\, K_{2\to2}\big(1'3' \to (13)_{out}\big).$$

where $K_{2\to2}$ is the block without two-particle states thus being up to factor the $K$-matrix function; hadrons are denoted by the indices $(1,3)$, the index 2 we keep for the centrally produced system, $(\ell\bar\ell)$ or $(Q\bar Q)$.

### 2.1.1 Impact parameter presentation

We consider the scattering amplitude in the cm-system where

$$p_1 \equiv (p_0, \mathbf{p}_\perp, p_z) = (p + m^2/2p, 0, p), \quad p_3 = (p + m^2/2p, 0, -p). \tag{4}$$

Therefore, we write:

$$\mathbf{k}_{1'\perp} + \mathbf{k}_{3'\perp} = 0, \quad \mathbf{k}_{1\perp} + \mathbf{k}_{3\perp} = 0. \tag{5}$$
$$q_{3'}^2 = (p_3 - k_{3'})^2 \simeq -\mathbf{k}_{3'\perp}^2, \quad q_{3'3}^2 = (k_{3'} - k_3)^2 \simeq -(\mathbf{k}_{3\perp} - \mathbf{k}_{3'\perp})^2.$$

The $K$-matrix function $(-i)K(b)$ of the scattering amplitude is real for the black disk regime. That means that the mass-on-shell contributions are dominant in the loop diagrams. For the rescattering diagrams this is realized by the replacement

$$\left[(m^2 - k_{1'}^2 - i0)(m^2 - k_{3'}^2 - i0)\right]^{-1} \to -2\pi^2\delta(m^2 - k_{1'}^2)\delta(m^2 - k_{3'}^2) = \tag{6}$$

$$-2\pi^2\delta\big(k_{1'}^{(+)}k_{1'}^{(-)} - (m^2 + \mathbf{k}_{1'\perp}^2)\big)\delta\big(k_{3'}^{(+)}k_{3'}^{(-)} - (m^2 + \mathbf{k}_{3'\perp}^2)\big),$$

where $k^{(+)} = k_0 + k_z, \quad k^{(-)} = k_0 - k_z$. Then the right-hand side of Eq. (3) reads:

$$A_{2\to2}(\mathbf{k}_{3\perp}^2, \ln s) = K_{2\to2}\big(\mathbf{k}_{3\perp}^2, \ln s\big) + \tag{7}$$

$$\int \frac{d^2 k_{3'\perp}}{(2\pi)^2}\, A_{2\to2}(\mathbf{k}_{3'\perp}^2, \ln s)\frac{i}{4s} K_{2\to2}\big((\mathbf{k}_{3'\perp} - \mathbf{k}_{3\perp})^2, \ln s\big),$$

where $K_{2\to2}/(4s)K$ is the $K$-matrix function in momentum representation. Correspondingly, the Fourier transform of it gives the $K$-matrix function in the impact parameter space:

$$\frac{1}{4s}K_{2\to2}\big(\mathbf{k}_\perp^2, \ln s\big) = \int d^2b \exp(i\mathbf{k}\mathbf{b})K(\mathbf{b}^2, \ln s),\tag{8}$$

$$\frac{i}{4s}A_{2\to2}\big(\mathbf{k}_\perp^2, \ln s\big) = \int d^2b \exp(i\mathbf{k}\mathbf{b})a(\mathbf{b}^2, \ln s),$$

Equation (7) in the impact parameter space is written as:

$$a(\mathbf{b}^2, \ln s) = iK(\mathbf{b}^2, \ln s) + a(\mathbf{b}^2, \ln s)\, iK(\mathbf{b}^2, \ln s).\tag{9}$$

Thus, we have the formula of the eikonal approach:

$$a(\mathbf{b}^2, \ln s) = \frac{iK(\mathbf{b}^2, \ln s)}{1 - iK(\mathbf{b}^2, \ln s)},\tag{10}$$

see Eq. (2). The function $K(\mathbf{b}^2, \ln s)$ depends on the energy and realizes effectively the instantaneous interaction which manifests itself in shrinking of diffractive cones with the energy increase.

### 2.1.2 Analytical properties of the diffractive scattering amplitude

The scattering amplitude has $t$-channel singularities at $t = (\sum m)^2$; for the $pp$ scattering they are $t = \mu_\pi^2$, $4\mu_\pi^2$, $9\mu_\pi^2$ and so on. All these singularities are effectively far from the region of consideration of the amplitude: at ultrahigh energies the amplitude depends on $\tau \sim |t|\ln^n s$ and the singularities in the $\tau$-plane tend to infinity with the energy increase, $\tau_{sing} = (\sum m)^2 \ln^n s \to \infty$. As a result, integrations over $k^{(+)}$, $k^{(-)}$ are factorized thus transforming the amplitude (3) into a set of loop diagrams:

$$a(\mathbf{b}^2, \ln s) = \sum_{\ell=1}^{\infty}\Big(iK(\mathbf{b}^2, \ln s)\Big)^\ell,\tag{11}$$

that reproduces (10).

The analytical properties in the $s$-plane are determined by the loop diagram and corresponding cut discontinuities - that are logarithmic terms, $A_{2\to2} \sim s\ln^N s$. At ultrahigh energies one should take into account the $u$-channel cut as well. For the positive signature we write $s\ln^N s + u\ln^N u = s\ln^N s + (-s)\ln^N(-s) \sim i\pi\ln^{N-1}$ that gives the dominant imaginary part. The choice of the $K(b)$ in accordance with Eq. (2) takes into account this property.

## 2.2 Black disk and resonant disk modes

We know that the profile function $T(b)$ reaches the black disk limit at small impact parameters, $b \lesssim 0.5\ fm$ at LHC energies. But it is not known whether $T(b)$ is frozen at $T(b) = 1$ or continues to increase with the energy growth [13]. Because of that we consider two versions for the asymptotic behavior: (i) with the black disk regime, $T(b) \to 1$ at $b < R_{disk}$, and (ii) with the maximal value of the profile function corresponding to the resonant disk regime, $T(b) \to 2$ at $b < R_{disk}$.
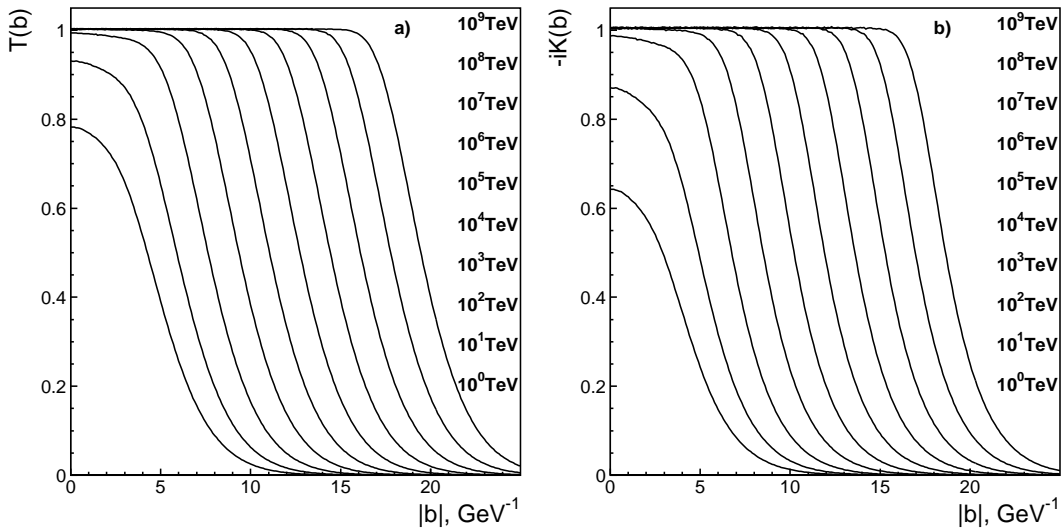
Figure 2: Black disk mode: a) Profile functions, $T(b)$, at $\sqrt{s} = 1, 10, 10^2, ...10^9$ TeV with $T(b) \to 1$ at $b < R \ln s$ and b) corresponding $K$-matrix function determined as $T(b) = -2iK(b)/[1 - iK(b)]$.

### 2.2.1 Black disk limit in terms of the Dakhno-Nikonov model

The Dakhno-Nikonov model [16] demonstrates us a representative example of application of the optical density technique for the consideration of $pp^{\pm}$ collisions at ultrahigh energies when $\ln s >> 1$. In the model the black disk is formed by the pomeron cloud and rescatterings are described within the eikonal approach. The same model may demonstrate the reformulation to the $K$-matrix technique.

The behavior of amplitudes at ultrahigh energies is determined by leading complex-j singularities, in the Dakhno-Nikonov model that are leading and next-to-leading pomerons with trajectories $\alpha(\mathbf{q}^2) \simeq 1 + \Delta - \alpha'\mathbf{q}^2$. The fit of refs. [11, 12] gives $\Delta = 0.27$ and $\alpha'_P = 0.12$ GeV$^{-2}$.

In terms of the $K$-matrix approach the black disk mode means the assumed freezing of the $-iK(b)$ in the interaction area:

$$\left[ -iK(b) \right]_{\xi \to \infty} \to 1 \qquad \text{at } b < R_0\,\xi\,, \tag{12}$$

$$\left[ -iK(b) \right]_{\xi \to \infty} \to 0 \qquad \text{at } b > R_0\,\xi\,,$$

$$\xi = \ln \frac{s}{s_R}, \quad s_R \simeq 6.4\ 10^3 \text{ GeV}^2, \quad \text{with } R_0 \simeq 2\sqrt{\alpha'\Delta} \simeq 0.08 \text{ fm.}$$

The growth of the radius of the black disk is slow: the small value of $R_0$ is caused by the large mass of glueballs [17, 18] and the effective mass of gluons [19, 20]. The black disk mode results in

$$\sigma_{tot} \simeq 2\pi(R_0\xi)^2, \tag{13}$$

$$\sigma_{el} \simeq \pi(R_0\xi)^2, \quad \sigma_{inel} \simeq \pi(R_0\xi)^2.$$

For the black disk radius the corrections of the order of $\ln \xi$ exist $R_{black\ disk} \simeq R_0\xi + \varrho \ln \xi$ but they become apparent in the Dakhno-Nikonov model at energies of the order of the Planck mass, $\sqrt{s} \sim 10^{17}$ TeV.
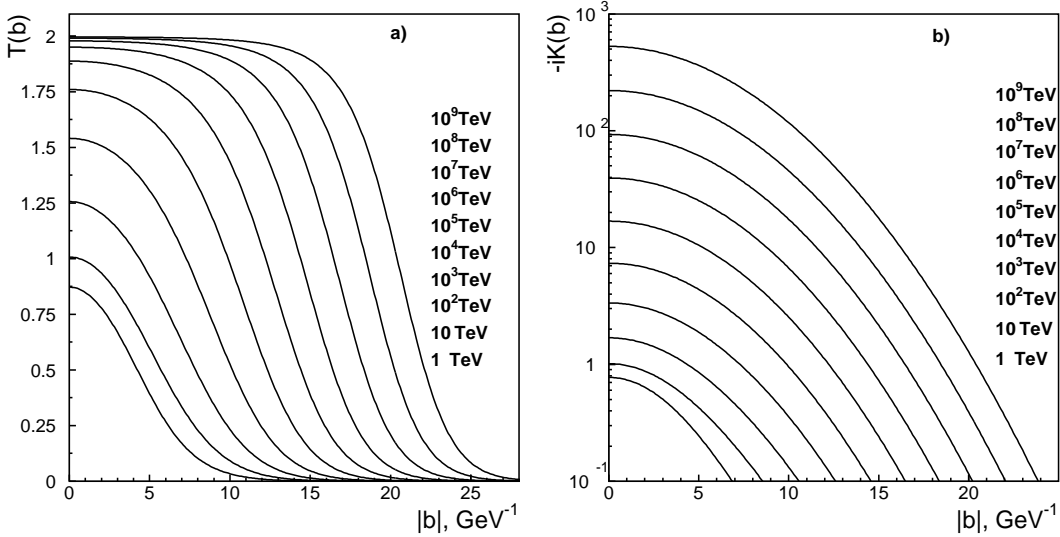
Figure 3: Resonant disk mode: a) the profile function $T(b)$ and b) $K$-matrix function, $-iK(b)$, $[-iK(b)]_{\xi \to \infty} \to \infty$ at $b < R_0\xi$.

### 2.2.2 Resonant disk and the $K$-matrix function growth

From the data it follows that both $T(b)$ and $-iK(b)$ are increasing with energy, being less than unity. If the eikonal mechanism does not quench the growth, both characteristics cross the black disk limit getting $T(b) > 1$, $-iK(b) > 1$. If $-iK(b) \to \infty$ at $\ln s \to \infty$, which corresponds to a growth caused by the supercritical pomeron ($\Delta > 0$), the diffractive scattering process gets to the resonant disk mode.

For following the resonant disk switch-on we use the two-pomeron model with parameters providing the description of data at 1.8 TeV and 7 TeV, namely:

$$-iK(b) = \int \frac{d^2q}{(2\pi)^2} \exp\left(-i\mathbf{q}\mathbf{b}\right) \sum g^2 s^\Delta e^{-(a+\alpha\xi)\mathbf{q}^2} \tag{14}$$

$$= \sum \frac{g^2}{4\pi(a+\alpha'\xi)} \exp\left[\Delta\xi - \frac{\mathbf{b}^2}{4(a+\alpha'\xi)}\right], \qquad \xi = \ln\frac{s}{s_0}.$$

The following parameters are found for the leading and the next-to-leading pomerons:

| parameters | leading pole | next-to-leading |
|---|---|---|
| $\Delta$ | 0.20 | 0 |
| $\alpha'_P$ [GeV$^{-2}$] | 0.18 | 0.14 |
| $a$ [GeV$^{-2}$] | 6.67 | 2.22 |
| $g^2$ [ mb ] | 1.74 | 28.6 |
| $s_0$ [GeV$^2$] | 1 | 1 |

(15)

The resonant interaction regime occurs at $b < 2\sqrt{\alpha'\Delta}\xi = R_{rd}\xi$, in this region $T(b) \to 2$. In terms of the inelasticity parameter and the phase shift it corresponds to $\eta \to 1$ and $\delta \to \pi/2$. Cross sections at $\xi \to \infty$ obey $\sigma_{tot} \simeq 4\pi R_{rd}^2\xi^2$, $\sigma_{el}/\sigma_{tot} \to 1$ and $\sigma_{inel} \simeq 2\pi R_{rd}\xi$.

At the energy $\sqrt{s} \sim 10$ TeV the cloud constituents fill out the proper hadron domain, the region $\leq 1$ fm, and that happens in both modes. It is demonstrated in Figs. 2a, 3a where

it is seen that the profile functions $T(b)$ coincide practically in both modes as well as the K-functions $-iK(b)$. Differences appeared at $\sqrt{s} \sim 1000$ TeV: $T(b) \simeq 1.5$ at $b \lesssim 0.5$ fm and the black zone has shifted to $b \simeq 1.0 - 1.5$ fm, Figs. 2b, 3b. With further energy increase the radius of the black band increases as $2\sqrt{\Delta\alpha'}\xi \equiv R_{rd}\xi$. The rate of growth in both modes is determined by the leading singularity and the fit of the data in the region $\sqrt{s} \sim 1 - 10$ TeV gives approximately the same values of $\Delta$ and $\alpha'$ for both cases thus providing $R_{rd} \simeq R_0$.

# 3 Production amplitude: screening effects due to initial and final state rescatterings

Return now to the productions of centrally produced particles, $\ell\bar{\ell}$ and $Q\bar{Q}$. The problem we solve is to calculate effects of the rescatterings presuming that the input amplitude is known. Therefore, we calculate an amplitude prolongation into the region of ultrahigh energies supposing we know the amplitude at lower energies. The evolution of the amplitude we calculate is determined by the growth of the hadron disk size, its long-range component.

### 3.0.3 Input amplitude for production of $\ell\bar{\ell}$ and $Q\bar{Q}$

The input amplitude for the production of three particles is shown in Fig. 1a, it is written as:

$$\phi_0(\mathbf{k}_1^2, \xi_{12}; \ \mathbf{k}_3^2, \xi_{23}) = \int d^2b_1 d^2b_3 f_0(b_1, \xi_{12}\ ; b_3\ , \xi_{23}) \exp\left(i\mathbf{k}_1\mathbf{b}_1 + i\mathbf{k}_3\mathbf{b}_3\right). \tag{16}$$

For the black disk mode we write the input term as:

$$\mathbf{k} - \text{space}: \quad \phi_0(\mathbf{k}_1^2, \xi_{12}; \ \mathbf{k}_3^2, \xi_{23}) = g_{2\to3} a(\mathbf{k}_1^2, \xi_{12})\, a(\mathbf{k}_3^2, \xi_{23})\,, \tag{17}$$

$$\mathbf{b} - \text{space}: \quad f_0(b_1, \xi_{12}\ ; b_3\ , \xi_{23}) = \frac{1}{4} g_{2\to3} T(b_1, \xi_{12})\, T(b_3, \xi_{23})$$

with $a(\mathbf{k}^2, \xi)$ and $T(b, \xi)$ being determined by Eq. (2).

In the resonant disk mode the diffractive processes are determined by pomeron-type exchanges, therefore we use the two-pomeron term. We write in the momentum and impact parameter spaces, correspondingly:

$$\mathbf{k} - \text{space}: \quad \phi_0(\mathbf{k}_1^2, \xi_{12}; \mathbf{k}_3^2, \xi_{23}) = g_{2\to3} \exp\left[\Delta\xi_{12} - \alpha'\xi_{12}\mathbf{k}_1^2\right] \exp\left[\Delta\xi_{23} - \alpha'\xi_{23}\mathbf{k}_3^2\right], \tag{18}$$

$$\mathbf{b} - \text{space}: \quad f_0(b_1, \xi_{12}\ ; b_3, \xi_{23}) = g_{2\to3} \frac{e^{\Delta\xi_{12}}}{4\pi\alpha'\xi_{12}} \exp\left[-\frac{\mathbf{b}_1^2}{4\alpha'\xi_{12}}\right] \frac{e^{\Delta\xi_{23}}}{4\pi\alpha'\xi_{23}} \exp\left[-\frac{\mathbf{b}_3^2}{4\alpha'\xi_{23}}\right].$$

### 3.0.4 Initial state rescatterings

Rescatterings in the initial state give additional terms into the production amplitude. The one-rescattering term reads:

$$\phi_1(\mathbf{k}_1^2, \xi_{12}; \ \mathbf{k}_3^2, \xi_{23}) = \int d^2b_1 d^2b_3\ iK(b, \xi) f_0(b_1, \xi_{12}\ ; b_3\ , \xi_{23}) \exp\left(i\mathbf{k}_1\mathbf{b}_1 + i\mathbf{k}_3\mathbf{b}_3\right),$$

$$\xi = \xi_{12} + \xi_{23}, \quad \mathbf{b} = \mathbf{b}_1 + \mathbf{b}_3. \tag{19}$$

In the impact parameter space the rescattering results in factor $iK(b, \xi)$. The two-rescatterings term contains the factor $(iK(b, \xi))^2$ and so on. The summation of all terms $\sum\limits_{n=0,1,2,...} f_n$ generates a standard $K$-matrix factor $(1 - iK(\xi, b))^{-1}$ and we write for the input term corrected by taking into account the initial state interactions:

$$\sum_{n=0}^{\infty} \phi_n(\mathbf{k}_1^2, \xi_{12}; \ \mathbf{k}_3^2, \xi_{23}) = \int d^2 b_1 d^2 b_3 \ \frac{1}{1 - iK(\xi, b)} f_0(b_1, \xi_{12} \ ; b_3 \ , \xi_{23}) \exp\left(i\mathbf{k}_1\mathbf{b}_1 + i\mathbf{k}_3\mathbf{b}_3\right). \quad (20)$$

The final state interactions lead to the same factor, and we have finally:

$$f(b_1, \xi_{12} \ ; b_3 \ , \xi_{23}) = \frac{f_0(b_1, \xi_{12} \ ; b_3 \ , \xi_{23})}{\left(1 - iK(b, \xi)\right)^2}. \quad (21)$$

Factor $\left(1 - iK(b, \xi)\right)^{-1}$ is universal for taking into account the rescattering corrections.

Rescattering corrections behave differently at ultrahigh energies: for the black disk mode $[1 - iK(b)]^{-1} \to 1/2$ at $\sqrt{s} \to \infty$ while for the resonant mode $[1 - iK(b)]^{-1} \to 0$ at $\sqrt{s} \to \infty$.

# 4  Generating operator for production amplitude

One can write Eq. (21) by the operator

$$f_0(b', \xi' \ ; b'', \xi'') \frac{\partial}{\partial\left(iK(b, \xi)\right)}, \quad (22)$$
$$\xi' + \xi'' = \xi, \quad \mathbf{b}' + \mathbf{b}'' = \mathbf{b}$$

acting on the scattering amplitude $a(\mathbf{b}^2, \xi)$ given in Eqs. (10), (11). For the reactions investigated here the generating operator looks as a plaything but it can be really helpful when the productions of the $\ell\bar{\ell}$ or $Q\bar{Q}$ pairs are considered in multihadron reactions like that studied in [14].

<center>***</center>

In terms of the modified $K$-matrix technique we consider central production $pp \to p(\ell\bar{\ell})p$ or $pp \to p(Q\bar{Q})p$ when momenta transferred to protons are small, $\mathbf{k}_\perp^2 \sim m^2/\ln^2 s$. Rescattering corrections, which are calculated in straightforward way, lead to substantial differences in energy behavior of production amplitudes at different modes, the black disk and resonant disk ones. In the resonant disk mode the scattering correction factor $[1 - iK(b)]^{-1}$ decreases with energy growth $[1 - iK(b)]^{-1} \to 0$ at $\sqrt{s} \to \infty$ while for the black disk mode $[1 - iK(b)]^{-1} \to 1/2$ at $\sqrt{s} \to \infty$; energy behavior differentials emphasize importance of studies of production processes.

# References

[1] G. Latino [on behalf of TOTEM Collaboration], EPJ Web Conf. **49**, 02005 (2013) [arXiv:1302.2098 [hep-ex]].

[2] ATLAS collaboration, G. Aad *et al.*, Eur. Phys. J. **C72** , 1926 (2012), arXiv:1201.2808 [hep-ph].

[3] CMS collaboration, *Measurement of diffraction dissociation cross sections at $\sqrt{s} = 7TeV$ at the LHC, CMS-PAS-FSQ-12-005,* 2013.

[4] ALICE collaboration, B. Abelev *et al.*, Eur. Phys. J. **C73** , 2456 (2013), arXiv:1208.4968 [hep-ph].

[5] Pierre Auger Collaboration (P. Abreu *et al.*), Phys. Rev. Lett. **109**, 062002 (2012).

[6] UA4 Collaboration, Phys. Lett. **B147** , 385 (1984);
UA4/2 Collaboration, Phys. Lett. **B316**, 448 (1993);
UA1 Collaboration, Phys. Lett. **B128**, 336 (1982);
E710 Collaboration, Phys. Lett. **B247**, 127 (1990);
CDF Collaboration, Phys. Rev. **D50**, 5518 (1994).

[7] F. Halzen, K. Igi, M. Ishida and C. S. Kim, Phys. Rev. **D85**, 074020 (2012) [arXiv:1110.1479 [hep-ph]].

[8] V. Uzhinsky and A. Galoyan, arXiv:1111.4984 [hep-ph].

[9] M. G. Ryskin, A. D. Martin and V. A. Khoze, Eur. Phys. J. **C72**, 1937 (2012) [arXiv:1201.6298 [hep-ph]].

[10] M. M. Block and F. Halzen, Phys. Rev. **D86**, 051504 (2012) [arXiv:1208.4086 [hep-ph]].

[11] V.V. Anisovich, K.V. Nikonov, and V.A. Nikonov, Phys. Rev. **D88**, 014039 (2013); [arXiv:1306.1735 (hep-ph)].

[12] V.V. Anisovich, V.A. Nikonov, and J. Nyiri, Phys. Rev. **D88**, 014039 (2013); [arXiv:1310.2839 (hep-ph)].

[13] V. V. Anisovich, V. A. Nikonov and J. Nyiri, arXiv:1408.0692 [hep-ph].

[14] V. V. Anisovich, M. A. Matveev and V. A. Nikonov, arXiv:1407.4588 [hep-ph].

[15] A.V. Anisovich, V.V. Anisovich, M.A. Matveev, V.A. Nikonov, J. Nyiri, A.V. Sarantsev *Three-particle physics and dispersion relation theory*, World Scientific, Singapore (2013).

[16] L.G. Dakhno and V.A. Nikonov, Eur. Phys. J. **A8**, 209 (1999).

[17] V.V. Anisovich, AIP Conf.Proc. **619**, 197 (2002), **717**, 441 (2004); Phys.Usp. **47**, 45 (2004), [UFN **47**, 49 (2004)].

[18] V.V. Anisovich, M.A. Matveev, J. Nyiri, A.V. Sarantsev, Int. J. Mod. Phys. **A20**, 6327 (2005).

[19] G. Parisi and R. Petronzio, Phys. Lett. **94**, 51 (1980).

[20] M. Consoli and J.H. Field, Phys. Rev. **D49**, 1293 (1994).